Title: **Particle Shape Effects on Packing Density, Stiffness and Strength –Natural and Crushed Sands-**

Authors: Gye-Chun Cho[1], Jake Dodds[2], and J. Carlos Santamarina[2]

[1] Assistant Professor, Civil and Environmental Engineering, Korea Advanced Institute of Science and Technology, 373-1, Guseong-dong, Yuseong-gu, Daejeon 305-701, Republic of Korea.
phone: 82-42-869-3622, fax: 82-42-869-3610, email: gyechun@kaist.edu

[2] Civil Engineer, National Resources Conservation Service, Price, Utah, USA
phone: 435-637-0041 (ext. 16), email: jake.dodds@ut.usda.gov

[3] Professor, Civil and Environmental Engineering, Georgia Institute of Technology, 790 Atlantic Drive, Atlanta, Georgia 30332-0355, USA.
phone: 1-404-894-7605, fax: 1-404-894-2281, email: carlos.santamarina@ce.gatech.edu

Document Summary

Number of Words: 4,266

Number of Tables: 2

Number of Figures: 11

PARTICLE SHAPE EFFECTS ON PACKING DENSITY, STIFFNESS AND STRENGTH

- NATURAL AND CRUSHED SANDS -

Gye-Chun Cho[1], Jake Dodds[2], and J. Carlos Santamarina[3]

ABSTRACT: The size and shape of soil particles reflect the formation history of the grains. In turn, the macroscale behavior of the soil mass results from particle level interactions which are affected by particle shape. Sphericity, roundness and smoothness characterize different scales associated to particle shape. New experimental data and data from previously published studies are gathered into two databases to explore the effects of particle shape on packing as well as small and large-strain properties of sandy soils. Data analysis shows that increased particle irregularity (angularity and/or eccentricity) leads to: an increase in e_{max} and e_{min}, a decrease in stiffness yet with increased sensitivity to the state of stress, an increase in compressibility under zero-lateral strain loading, and an increase in critical state friction angle ϕ_{cs} and intercept Γ with a weak effect on slope λ. Therefore, particle shape emerges as a significant soil index property that needs to be properly characterized and documented, particularly in clean sands and gravels. The systematic assessment of particle shape will lead to a better understanding of sand behavior.

KEYWORDS: angularity; compression index; critical state parameters; friction angle; particle shape; roundness; sands; small strain stiffness; sphericity; strength.

---

[1] Assistant Professor, Civil & Environ. Eng., KAIST, Daejeon, Korea
[2] Civil Engineer, National Resources Conservation Service, Price, Utah, USA
[3] Professor and Goizueta Chair, Civil & Environ. Eng., Georgia Institute of Technology, Atlanta, Georgia, USA

INTRODUCTION

Particle size and shape reflect material composition, grain formation and release from the mineral matrix, transportation, and depositional environments. Mechanical and chemical processes determine grain shape once it is released from the matrix (Margolis and Krinsley 1974, Rahaman 1995). The transition region from chemical to mechanical shape-control occurs for a particle size between d~50-to-400 μm. Chemical action and abrasion increase with age and older sands tend to be rounder regardless of particle size. The larger the particle the higher the probability of imperfections and brittle fracturing (typically d>400μm). Conversely, smaller particles are stronger by lack of imperfections, then, failure by cleavage along crystal atomic planes becomes energetically advantageous and the resulting particles are more platy (Margolis and Krinsley 1974). High-coordination conditions (rather than a diametrically loaded isolated particle) promotes the splitting of elongated particles (i.e., increased cubicity) and shear abrasion.

Particle shape is characterized by three dimensionless ratios (Wadell 1932, Krumbein 1941, Powers 1953, Krumbein and Sloss 1963, Barrett 1980): *sphericity S* (cf. eccentricity or platiness), *roundness R* (cf. angularity) and *smoothness* (cf. roughness). Sphericity indicates whether one, two, or three of the particle dimensions are of the same order of magnitude, and it is defined as the diameter of the largest inscribed sphere relative to the diameter of the smallest circumscribed sphere. Roundness is quantified as the average radius of curvature of surface features relative to the radius of the maximum sphere that can be inscribed in the particle. Roughness describes the surface texture relative to the radius of the particle. Spehricity, roundness and smoothness form an independent set. While sphericity and roundness increase by abrasion, they do not increase proportionally. Furthermore, chipping of a particle may increase the sphericity, but it decreases the roundness (Wadel 1932). Perfectly round particles can have non-spherical shape (e.g., elliptical particles or disk particles) and equidimensional particles can be very angular (e.g., cube or

hexahedron).

The macroscale behavior of soils results from particle level characteristics and processes. Specifically, it is intuitively recognized that particle shape affects soil behavior (for a general review see Santamarina and Cho 2004). However, a comprehensive confirmatory study is lacking. Furthermore, geotechnical soil classification systems -including the USCS- do not take particle shape into consideration. Therefore, the true role of particle shape on soil response remains vague.

The primary purpose of this study is to gather data that permit investigating the role of particle shape on index properties, small strain stiffness and large-strain critical state parameters of natural and crushed sands. Later, we explore correlations between index properties and mechanical parameters that are justified by particle shape. This study addresses sphericity and roundness only (previous studies on the effects of roughness can be found in Santamarina and Cascante 1998, Yimsiri and Soga 1999).

DATABASES - TEST PROCEDURES

The main database developed for this study is designed to study the effect of particle shape on soil properties (this database is summarized in Table A1 - additional details can be found in Cho 2001 and Dodds 2003). Most of the data are experimentally obtained as part of this research (data from Sukumaran and Ashmawy 2001, Ashmawy et al. 2003 are included as noted). The tested soils include 17 crushed sands from Georgia (granite and carbonate) and 16 natural sands from various places around the world, and some other materials such as glass beads, granite powder and Syncrude tailings. The measured parameters are: roundness, sphericity, grain size distribution, extreme void ratios e_{max} and e_{min}, small strain shear wave velocity as a measure of G_{max}, compression and swelling indices under zero-lateral strain loading, and critical state parameters.

Particle size and extreme void ratios e_{max} and e_{min} are obtained following standard procedures (ASTM C136 D4254, and D1557). The methodology used to obtain other parameters are presented in the following section.

A second database is compiled from published experimental results (this database is summarized in Table A2). In general, particle shape is not documented in the literature, therefore, this database is used to complement the main database when exploring expected shape-dependent correlations between soil index properties and critical state parameters. The following soil index properties are known for this database: mean grain size D_{50} [mm], coefficient of uniformity C_u, maximum void ratio e_{max}, minimum void ratio e_{min}, and fines content (percentage by weight passing sieve #200).

Particle Shape

Sphericity and roundness can be effectively characterized by visual comparison with charts (Folk 1955, Barrett 1980). Digital image analysis facilitates the evaluation of mathematical descriptors of particle shape including Fourier analysis, fractal analysis and other hybrid techniques (e.g., Meloy 1977, Clark 1987, Hyslip and Vallejo 1997, Bowman et al. 2001, Sukumaran and Ashmawy 2001). The direct measurement of roughness is cumbersome: the fractal nature of rough surfaces implies that there is no characteristic scale on the surface itself. Therefore, the relevant observation length of roughness becomes the interparticle contact area: this is what a particle "sees" in its neighbor. Finally, shape parameters can be inferred from macro-scale behavior of the soil mass. For instance, particle shape affects granular flow on inclined planes, residence time on sieves, and sedimentation time in a fluid column. However, it is not possible to separate the relative contributions of roughness, sphericity and roundness from such individual measurements.

In this study, sphericity and roundness are determined using the chart shown in Fig. 1. For a given

sand, grains are studied at various magnifications (Leica MZ6 stereomicroscope). Then the sphericity and roundness of representative grains are determined by comparing shapes in 2D photographs with those in the chart shown in Fig. 1. Regularity ρ is computed as the average between roundness and sphericity, $\rho = (R+S)/2$. Fig. 2 shows microphotographs of selected grains encountered in this study.

Most crushed sands exhibit similar shapes: roundness near R=0.2-to-0.3 and sphericity around S=0.7-to-0.8. Shape varies with particle size and smaller particles are more planar and with sharper corners. Crushed sands contain between 1% and 25% of platy mica particles. Natural sands exhibit a wider range of shapes; typically: roundness R=0.3-to-0.9 and sphericity S=0.5-to-0.9. Margaret river sand has very smooth texture while Ponte Vedra and Jekyll Island sands contain a significant percentage of platy crushed shells.

Small Strain Stiffness During Zero-Lateral Strain Loading

The effect of particle shape on small strain and oedometric stiffness is studied by measuring shear wave velocity during specimen loading and unloading in an oedometeric cell fitted with bender elements. Six natural sands and ten crushed sands are tested. All specimens are prepared dense (D_r=80-to-90%) by tamping each layer with a 32 mm diameter rod, starting at the outside and moving towards the center. The 100 mm diameter specimens are loaded with 2.8, 6.9, 13.7, 27.5, 55, and 110 N at 10-minute intervals then unloaded in the same manner. Dial gauge readings and shear wave signals are recorded prior to the next load step. Figs. 3 and 4 present typical load deformation data and received signals. The compression and expansion indices C_c and C_s are determined for the 30-to-300 kPa load interval for each sand (Table A1).

Critical State Parameters

Critical state soil behavior captures the large-strain behavior of soils in terms of shear stress $q=(\sigma_1-\sigma_3)$, mean effective stress $p'=(\sigma'_1+2\sigma'_3)/3$, and void ratio e. The critical state line CSL is the loci of critical state conditions in the e-p'-q space (Roscoe *et al*. 1958, Schofield and Wroth 1968, Wood 1990). Its projection on the p'-q space defines the strength parameter M

$$\mathrm{M} = \frac{q_{cs}}{p'_{cs}} = \frac{6\sin\phi_{cs}}{3-\sin\phi_{cs}} \tag{1}$$

where the subindex CS denotes critical state. The second term applies to axisymmetric, axial compression, and it is a function of the constant volume critical state friction angle ϕ_{cs}. The projection of the critical state line onto the e-log p' space defines the slope λ and intercept Γ,

$$e_{cs} = \Gamma - \lambda \log\left(\frac{p'_{cs}}{1kPa}\right) \tag{2}$$

The determination of critical state parameters is affected by localization and limited strain level. Both difficulties are overcome in this study by subjecting homogeneous contractive specimens to drained axial loading to large strains, following the simplified procedure suggested in Santamarina and Cho (2001). Critical state parameters are corroborated for selected soils running drained triaxial tests on otherwise similar homogeneous and contractive specimens.

RESULTS AND ANALYSES: SHAPE AND SOIL PROPERTIES

All measured values are summarized in Table A1. The wide range of material parameters permits gaining insight into the effect of particle shape on natural and crushed sands. A comprehensive analysis of particle shape effects in different strain regimes follows.

Packing

The effect of particle shape on maximum and minimum void ratios is explored in Fig. 5. Both e_{max} and e_{min}, and the void ratio difference $I_e = e_{max}$-e_{min} increase as roundness and sphericity decrease. Similar observations can be found in Fraser (1935), Shimobe and Moroto (1995), Miura et al. (1998), Cubrinovski and Ishihara (2002), Dyskin et al. (2001), and Jia and Williams (2001). Clearly, irregularity hinders particle mobility and their ability to attain minimum potential energy configurations. In the extreme case of low-sphericity, platy mica particles bridge gaps between grains and create large open voids (Guimaraes 2002). The relevance of grain size distribution and the coefficient of uniformity C_u on packing density is purposely removed from this figure, where all soils have $C_u \leq 2.5$ (see Youd 1973).

The simple cubic packing is the loosest stable packing that can be obtained with mono-sized spherical particles (coordination number cn=6, void ratio e=0.91, porosity n=0.48), while the tetrahedral or pyramidal packing is the densest (cn=12, e=0.34, n=0.26). Two extreme configurations are "geometrically stretched" to explore the effect of sphericity on extreme packing densities; results are shown in Fig. 6: as sphericity decreases, the range of attainable porosities increases, in agreement with Fig. 5(b). The predicted extreme configurations are attained with the aid of electrical interparticle forces or compliant particles such as clays; in the case of coarse and rigid sand grains data show lower variability than the theoretically predicted bounds.

Small Strain Behavior - Stiffness

The small-strain stiffness of a soil is measured by imposing a smaller strain than the elastic threshold strain γ_e (typically $\gamma_e < 10^{-4}$ in sands). In this case, the granular skeleton deforms at

constant fabric experiencing contact level deformation only. Therefore, the small-strain shear stiffness G_{max} of a soil reflects the nature of interparticle contacts, e.g., Hertzian deformation between two smooth spherical particles. The resulting non-linear stress-dependent stiffness $G_{max}=a\sigma'^{b}$ is captured in the shear wave velocity $V_s=\sqrt{(G/\rho)}$, through velocity-stress relations of the form

$$V_s = \alpha\left(\frac{\sigma'_{mean}}{1kPa}\right)^{\beta} \tag{3}$$

where the factor α [m/s] is the shear wave velocity at 1kPa and the exponent β reflects the sensitivity of the shear wave velocity to the mean state of stress σ'_{mean} in the shear plane.

Examples of shear wave velocity variation with effective confining stress are shown in Fig. 7 (for the same two sands selected for Figs. 3 and 4). The α-factor and the β-exponent are obtained by fitting Eq. (3) to loading data (computed values are summarized in Table A1). The effect of particle shape on small-strain shear wave parameters α and β are explored in Fig. 8: as sphericity and roundness decrease, the value of α decreases while β increases. This inverse relationship between α, the velocity at 1kPa, and β, the sensitivity to the state of stress, has been previously observed for a wide range of soils and it is further corroborated in Fig. 8(e). These results show that the sensitivity of stiffness to state of stress increases as particle shape becomes angular and less spherical. Increased roughness and increased percentage of platy mica particles have similar effects α and β (Santamarina and Cascante 1998, Guimaraes 2002)

Intermediate Strain Behavior – Zero-Lateral Strain Loading

Sand deformation under zero lateral strain loading may exceed the elastic threshold strain γ_e and new particle-scale deformation mechanisms take place, including contact slippage (facilitated in

smooth particles), breakage at contacts (intensified by angularity) and ensuing fabric changes. The effect of particle shape on oedometric modulus determined at zero-lateral strain is explored using the experimental data in Table A1. Fig. 9 shows that increased particle regularity leads to lower compression and swelling indices.

Large Strain Behavior – Critical State

Large strain soil behavior involves particle rotation and contact slippage. At low density, the interparticle coordination is low, shear deformation causes particle rotation and chain buckling, and the packing gradually densifies. However, rotation is frustrated in dense soils with high interparticle coordination, therefore, energy applied during shear loading is consumed either in dilation (to reduce coordination number) or in frictional slippage at contacts. Energy minimization dictates the interplay between these mechanisms, the statistical equilibrium at critical state and the evolution of anisotropy during shear. Ultimately, the shear strength of a soil reflects its ability to develop internal force and fabric anisotropy (Rothenburg and Bathurst 1989, Thornton 2000).

Within this particle-level mechanical framework, it is appropriate to hypothesize that eccentricity, angularity and roughness add difficulty to particle rotation, enhance dilatancy and the evolution of anisotropy i.e., greater shear resistance. This hypothesis is tested against experimental test results summarized in Fig. 10. The three critical state parameters Γ, λ and ϕ_{cs} decrease with increasing roundness, sphericity and overall regularity. Roundness is more relevant to critical state friction angle ϕ_{cs} and intercept Γ than sphericity, and the following guidelines are obtained

$$\phi_{cs} = 42 - 17R \tag{4}$$

$$\Gamma = 1.2 - 0.4R \tag{5}$$

The slope λ is poorly defined by shape parameters. However, the critical state void ratio e_{cs100} at a

mean principal stress p'= 100kPa, computed as e_{cs100}=Γ-2λ (Eq. 2), exhibits good correlation with particle regularity ρ (Fig. 10-d):

$$e_{cs100} = 1.1 - 0.42\rho \quad (6)$$

Clearly, the constant volume critical state friction angle ϕ_{cs} is not just dependent on mineral-to-mineral friction but strongly affected by particle shape (see also Chan and Page 1997).

SHAPE-DEPENDENT PARAMETER CORRELATION

The particle shape dependency exhibited by grain packing (extreme void ratios e_{max} and e_{min}) and by mechanical parameters (V_s, C_c, C_s, Γ, λ and ϕ_{cs}) suggests correlations among these parameters through particle shape effects. This is investigated by combining the experimental data gathered in this study (Table A1 - includes particle shape) and data gathered from the literature (Table A2 - does not include particle shape).

The critical state fabric is not expected to resemble the fabric a soil develops during e_{max} measurements by funneling or during particle rearrangement during e_{min} determinations. However, stability conditions at the particle-level are controlled by similar particle characteristics. Therefore, correlations between Γ (e_{cs} at p'=1kPa) and the critical state void ratio at p'=100 kPa (e_{cs100}=Γ-2λ) with extreme void ratios e_{max} and e_{min} are expected. Fig. 11(a&b) show that both Γ and e_{cs100} increase when extreme void ratios increase, in relation to decreased particle regularity. The intercept Γ trails e_{max}, while e_{cs100} corresponds to a relative density typically lower than D_r=50%.

Weak correlations are found between the critical state friction angle ϕ_{cs} or the slope of the critical state line λ with index properties e_{max}, e_{min} or I_e. Fig. 11(c) shows λ-vs-I_e and the underlying role of particle shape. By definition, the slope of the critical state line is $\lambda = \Delta e_{cs}/\Delta p'_{cs}$, therefore, it should

reflect the potential range in void ratios a soil may attain $I_e=e_{max}-e_{min}$. Published critical state parameters may have been obtained from specimens that experienced localization (localization was prevented in the tests conducted as part of this research). While localization affects Γ and λ, it has virtually no effect on ϕ_{cs} (Santamarina and Cho 2004).

Fig. 11(d) presents measured values of e_{max} vs. the predicted values computed taking into consideration e_{min} and the coefficient of uniformity C_u according to the following regression equation:

$$e_{max} = 1.35 e_{min} + 0.15(C_u - 1) \quad (7)$$

The plot shows the segregation of the data according to particle shape. The inverted equation highlights the importance that the coefficient of uniformity has on packing.

CONCLUSIONS AND RECOMMENDATIONS

Soils are made of grains. Grain size distribution plays a pivotal role in determining soil behavior. However, particle shape emerges as a significant parameter.

The shape of grains is established at three different scales: the global form, the scale of major surface features and the scale of surface roughness. Each scale reflects aspects of the formation history, and participates in determining the global behavior of the soil mass from particle packing to mechanical response. The direct measurement of particle surface roughness is cumbersome and its effects remain poorly known.

The increase in particle irregularity (angularity and/or eccentricity) leads to:

- increase in e_{max} and e_{min}, and $I_e=e_{max}-e_{min}$,
- decrease in stiffness (α coefficient), yet increased sensitivity to the state of stress (β

exponent)

- increase compressibility under zero-lateral strain loading (C_c)
- increase constant volume critical state friction angle ϕ_{cs} and intercept Γ (weak effect on slope λ)

The systematic assessment of particle shape will lead to a better understanding of sand behavior. In the meantime, it is recommended that particle shape be characterized and explicitly documented as part of every soil characterization exercise, in particular for soils that fall under the following USCS denominations: GW, GP, SW and SP.

ACKNOWLEDGMENTS

Support was provided by NSF (project on scales), the Georgia Mining Industry, The Goizueta Foundation, and the Smart Infra-Structure Technology Center (SISTeC) under KOSEF.

REFERENCES

Arulanandan, K., Seed, H.B., Yogachandran, C., Muraleetharan, K.K., and Seed, R.B. (1993). "Centrifuge study on volume changes and dynamic stability of earth dams." *Journal of Geotechnical Engineering*, ASCE, 119(11), 1717-1731.

Ashmawy, A.K., Sukumaran, B., and Vinh Hoang, V. (2003). "Evaluating the influence of particle shape on liquefaction behavior using discrete element modelling." *Annual International Society of Offshore and Polar Engineering Conference*, Hawaii, USA, PCW-05.

Barrett, P.J. (1980). "The shape of rock particles, a critical review." *Sedimentology*, 27, 291-303.

Been, K., and Jefferies, M.G. (1985). "A state parameter for sands." *Géotechnique*, 35(2), 99-112.

Been, K., Jefferies, M.G., and Hachey, J. (1991). "The critical state of sands." *Géotechnique*, 41(3), 365-381.

Bowman, E.T., Soga, K., and Drummnond, W. (2001). "Particle shape characterization using Fourier descriptor analysis." *Géotechnique*, 51(6), 545-554.

Castro, G., Enos, J.L., France, J.W., and Poulos, S.J. (1982). "Liquefaction induced by cyclic loading." *Report to National Science Foundation*, Washington, DC, No. NSF/CEE-82018.

Chan, L.C.Y. and Page, N.W. (1997). "Particle fractal and load effects on internal friction in powders." *Powder Technology*, 90, 259-266.

Chen, Y.C., and Liao, T.S. (1999). "Studies of the state parameter and liquefaction resistance of sands." *Earthquake Geotechnical Engineering*, Seco e Pinto (ed.), 513-518.

Chillarige, A.V., Robertson, P.K., Morgenstern, N.R., and Christian, H.A. (1997). "Evaluation of the in situ state of Fraser River sand." *Canadian Geotechnical Journal*, 34, 510-519.

Cho, G.C. (2001). *Unsaturated Soil Stiffness and Post-liquefaction Shear Strength*, Ph.D. Thesis, Georgia Institute of Technology, Atlanta, 288 pages.

Chu, J., and Lo, S.C.R. (1993). "On the measurement of critical state parameters of dense granular soils." *Geotechnical Testing Journal*, 16(1), 27-35.

Clark, N.N. (1987). "A new scheme for particle shape characterization based on fractal harmonics and fractal dimensions." *Powder Technology*, 51, 243-249.

Cubrinovski, M. and Ishihara, K. (2002). "Maximum and minimum void ratio characteristics of sands." *Soils and Foundation*, 42(6), 65-78.

Cunning, J.C., Robertson, P.K., and Sego, D.C. (1995). "Shear Wave Velocity to Evaluate in situ State of Cohesionless Soils." *Canadian Geotechnical Journal*, 32, 848-858.

Dobry, R., Vasquez-Herrera, A., Mohamad, R., and Vucetic, M. (1985). "Liquefaction flow failure of silty sand by torsional cyclic tests." *Advances in the art of testing soils under cyclic conditions*, Proceedings of a session sponsored by the Geotechnical Engineering Division in conjunction with the ASCE Convention in Detroit, Michigan, Khosla (ed.), 29-50.

Dodds J.S. (2003), Particle Shape and Stiffness - Effects on Soil Behavior, MSc Thesis, Georgia Institute of Technology, Atlanta, 173 pages.

Dyskin, A.V., Estrin, Y., Kanel-Belov, A.J., and Pasternak, E. (2001). "Toughening by fragmentation—How topology helps." *Advanced Engineering Materials*, 3(1), 885-888.

Folk, R.L. (1955). "Student operator error in determination of roundness, sphericity, and grain size." *Journal of Sedimentary Petrology*, 25(4), 297-301.

Fraser, H.J. (1935). "Experimental study of the porosity and permeability of clastic sediments." *Journal of Geology*, 13(8), 910-1010.

Gajo, A., and Wood, M. (1999). "A kinematic hardening constitutive model for sands: the multiaxial formulation." *International Journal for Numerical and Analytical Methods in Geomechanics*, 23, 925-965.

Guimaraes, M. (2002). *Crushed stone fines and ion removal from clay slurries - fundamental studies*, PhD thesis, Georgia Institute of Technology, Atlanta, 238 pages.

Hyslip, J.P. and Vallejo, L.E. (1997). "Fractal analysis of the roughness and size distribution of granular materials." *Engineering Geology*, 48, 231-244.

Ishihara, K. (1993). "The Rankine Lecture: Liquefaction and flow failure during earthquakes." *Géotechnique*, 43(3), 351-415.

Jia, X. and Williams, R.A. (2001). "A packing algorithm for particles of arbitrary shapes." *Powder Technology*, 120, 175-186.

Konrad, J.M. (1990). "Minimum undrained strength versus steady-state strength of sands." *Journal of Geotechnical Engineering*, 116(6), 948-963.

Konrad, J.M., and Watts, B.D. (1995). "Undrained shear strength for liquefaction flow failure analysis." *Canadian Geotechnical Journal*, 32, 783-794.

Konrad, J.M. (1997). "Insitu sand state from CPT: evaluation of a unified approach at two CANLEX sites." *Canadian Geotechnical Journal*, 34(1), 120-130.

Krumbein, W.C. (1941). "Measurement and geological significance of shape and roundness of sedimentary particles." *Journal of Sedimentary Petrology*, 11(2), 64-72.

Krumbein, W.C. and Sloss, L.L. (1963). *Stratigraphy and Sedimentation*, Second Edition, W.H. Freeman and Company, San Francisco, 660 pages.

Lee, C.J. (1995). "Static shear and liquefaction potential of sand." Proceedings of 3rd International Conference on Recent Advances in Geotechnical Earthquake Engineering and Soil Dynamics, St. Louis, Missouri, April 2-7, 1, 115-118.

Margolis, S.V. and Krinsley, D.H. (1974). "Processes of formation and environmental occurrence of microfeatures on detrital quartz grains." *American Journal of Science*, 274, 449-464.

Meloy, T.P. (1977). "Fast Fourier transforms applied to shape analysis of particle silhouettes to obtain morphological data." *Powder Technology*, 17, 27-35.

Miura, K., Maeda K., Furukawa, M., Toki, S. (1998). "Mechanical characteristics of sands with different primary properties." *Soils and Foundations*, 38, 159-172.

Powers, M.C. (1953). "A new roundness scale for sedimentary particles." *Journal of Sedimentary Petrology*, 23(2), 117-119.

Rahaman, M.N. (1995). *Ceramic Processing and Sintering*, Dekker Inc., NY, 770 pages.

Riemer, M.F., and Seed, R.B. (1997). "Factors affecting apparent position of steady-state line." *Journal of Geotechnical and Geoenvironmental Engineering*, 123(3), 281-288.

Riemer, M.F., Seed, R.B., Nicholson, P.G. and Jong, H.L. (1990). "Steady state testing of loose sands: limiting minimum density." *Journal of Geotechnical Engineering*, ASCE, 116(2), 332-337.

Robertson, P.K., Sasitharan, S., Cunning, J.C., and Sego, D.C. (1995). "Shear-Wave Velocity to Evaluate In-Situ State of Ottawa Sand." *Journal of Geotechnical Engineering*, 121(3), 262-273.

Roscoe, K.H., Schofield, A.N., Wroth, C.P. (1958). "On the yielding of soils." *Géotechnique*, 8, 22-53.

Rothenburg, L. and Bathurst, R.J. (1989). "Analytical study of induced anisotropy in idealized granular

material." *Géotechnique*, 49, 601-614.

Santamarina, J.C., and Cascante, G. (1998). "Effect of surface roughness on wave propagation parameters." *Géotechnique*, 48(1), 129-137.

Santamarina, J.C., and Cho, G.C. (2001). "Determination of critical state parameters in sandy soils – simple procedure." *Geotechnical Testing Journal*, GTJODJ, 24(2), 185-192.

Santamarina, J.C., and Cho, G.C. (2004). "Soil behaviour: The role of particle shape." *Advances in Geotechnical Engineering: The Skempton Conference*, R.J. Jardine et al. (ed.), 29-31 March 2004, Thomas Telford, London, 1, 604-617.

Sasitharan, S., Robertson, P.K., Sego, D.C., and Morgenstern, N.R. (1994). "State-boundary surface for very loose sand and its practical implications." *Canadian Geotechnical Journal*, 31, 321-334.

Schofield, A.N., and Wroth, P. (1968). *Critical State Soil Mechanics*, McGraw-Hill Book Company.

Shimobe, S., and Moroto, N. (1995). "A new classification chart for sand liquefaction." *Earthquake Geotechnical Engineering*, K. Ishihara (ed.), Balkema, Rotterdam, 315-320.

Sladen, J.A., and Handford, G. (1987). "A potential systematic error in laboratory testing of very loose sand." *Canadian Geotechnical Journal*, 24, 462-466.

Sladen, J.A., D'Hollander, R.D., and Krahn, J. (1985). "The liquefaction of sands, a collapse surface approach", *Canadian Geotechnical Journal*, 22, 564-578.

Sukumaran, B., and Ashmawy, A.K. (2001). "Quantitative characterization of the geometry of discrete particles." *Géotechnique*, 51(7), 171-179.

Thevanayagam, S., Wang, C.C., and Ravishankar, K. (1996). "Determination of post-liquefaction strength: steady state vs residual strength." *Uncertainty in the Geological Environment: from theory to practice*, Proceedings of Uncertainty '96, Schackelford et at. (ed.), Geotechnical Special Publication No. 58, 2, 1210-1224.

Thornton, C. (2000). "Numerical simulations of deviatoric shear deformation of granular media."

Géotechnique, 50(1), 43-53.

Toki, S., Tatsuoka, F., Miura, S., Yoshimi, Y., Yasuda, S., and Makihara, Y. (1986). "Cyclic undrained triaxial strength of sand by a cooperative test program." *Soils and Foundations*, 26(3), 117-128.

Verdugo, R., Castillo, P., and Briceno, L. (1995). "Initial Soil Structure and Steady-State Strength." *The First International Conference on Earthquake Geotechnical Engineering*, K. Ishihara (ed.), Balkema, 1, 209-214.

Wadel, H. (1932). "Volume, shape, and roundness of rock particles." *Journal of Geology*, 40, 443-451.

Wood, D.M. (1990). *Soil behavior and critical state soil mechanics*, Cambridge University Press, Cambridge, UK.

Yimsiri, S. and Soga, K. (1999). "Effect of surface roughness on small-strain modulus: micromechanics view." *Pre-failure Deformation Characteristics of Geomaterials: Proceedings*, *2nd International Symposium*, M. Jamiolkowski et al. (ed.), Torino, Italy, 597-602

Youd, T.L. (1973). "Factors controlling maximum and minimum densities of sands." *Evaluation of Relative Density and Its Role in Geotechnical Projects Involving Cohesionless Soils*, ASTM STP 523, American Society For Testing and Materials, 98-112.

Zhang, H., and Garga, V.K. (1997). "Quasi-Steady State: a real behaviour?" *Canadian Geotechnical Journal*, 34, 749-761.

LIST OF FIGURES

LIST OF TABLES IN APPENDIX

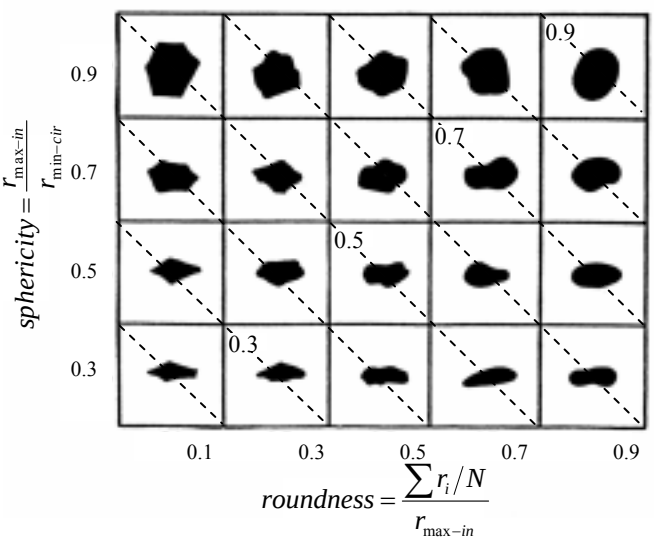

Fig. 1. Sphericity *S* and roundness *R* chart. Diagonal dotted lines correspond to constant particle regularity ρ=(*R*+*S*)/2 (modified from Krumbein and Sloss 1963).

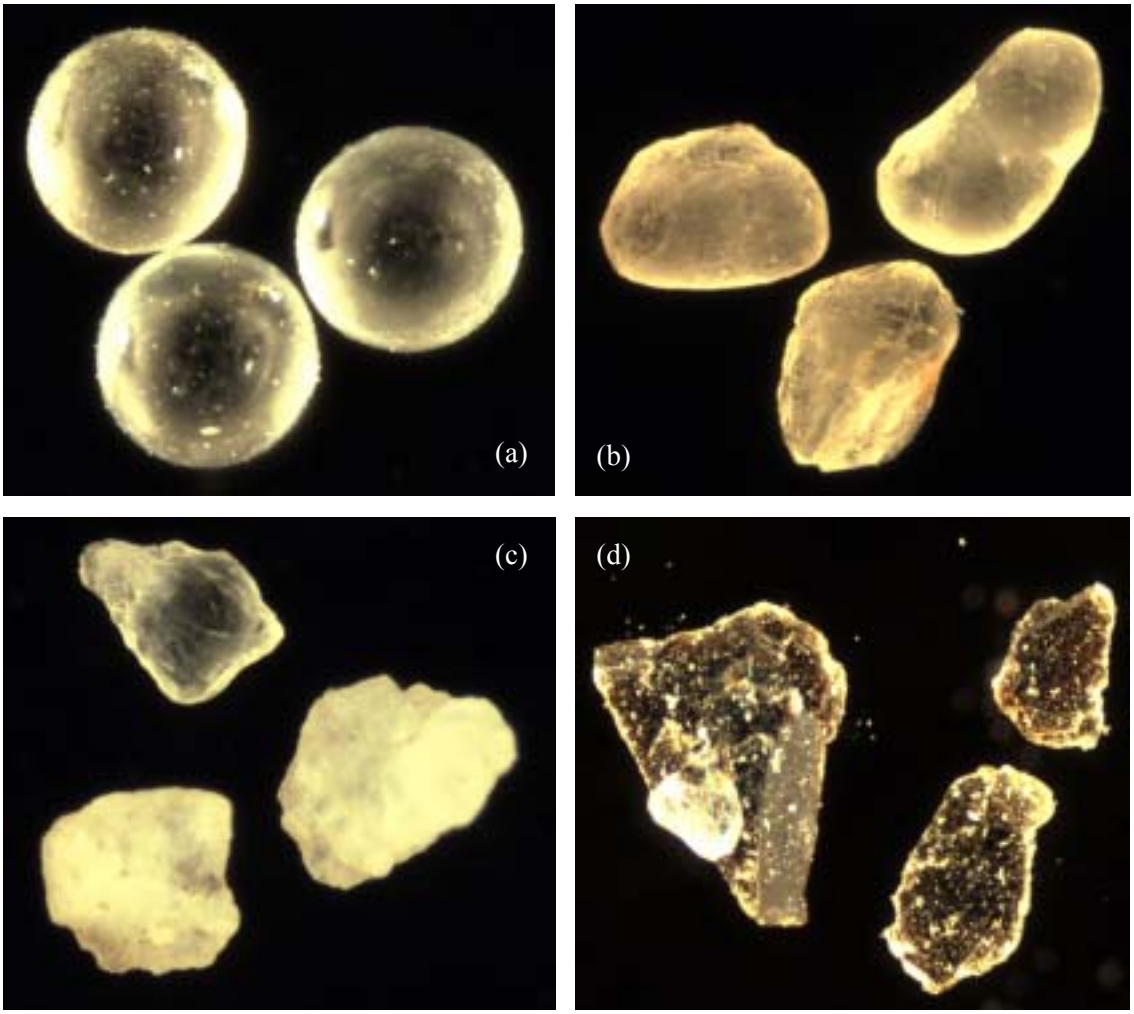

Fig. 2. Microphotographs of typical grains tested in this study. (a) Glass beeds D_{50}= mm. (b) Ottawa sand D_{50}=0.60 mm. (c) Ticino sand D_{50}= 0.33 mm. (d) Fine fraction of crushed sands D≈ 0.08 mm.

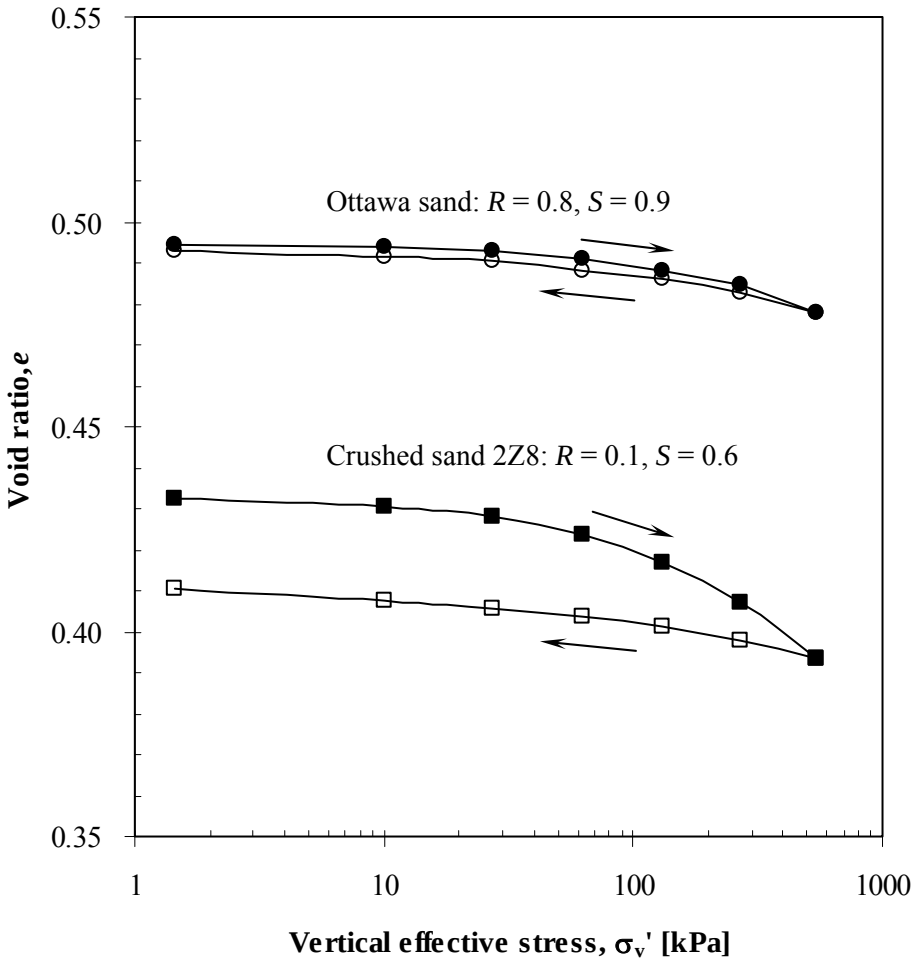

Fig. 3. The variation of void ratio with vertical effective stress during zero-lateral strain loading (additional properties for these sands can be found in Table A1).

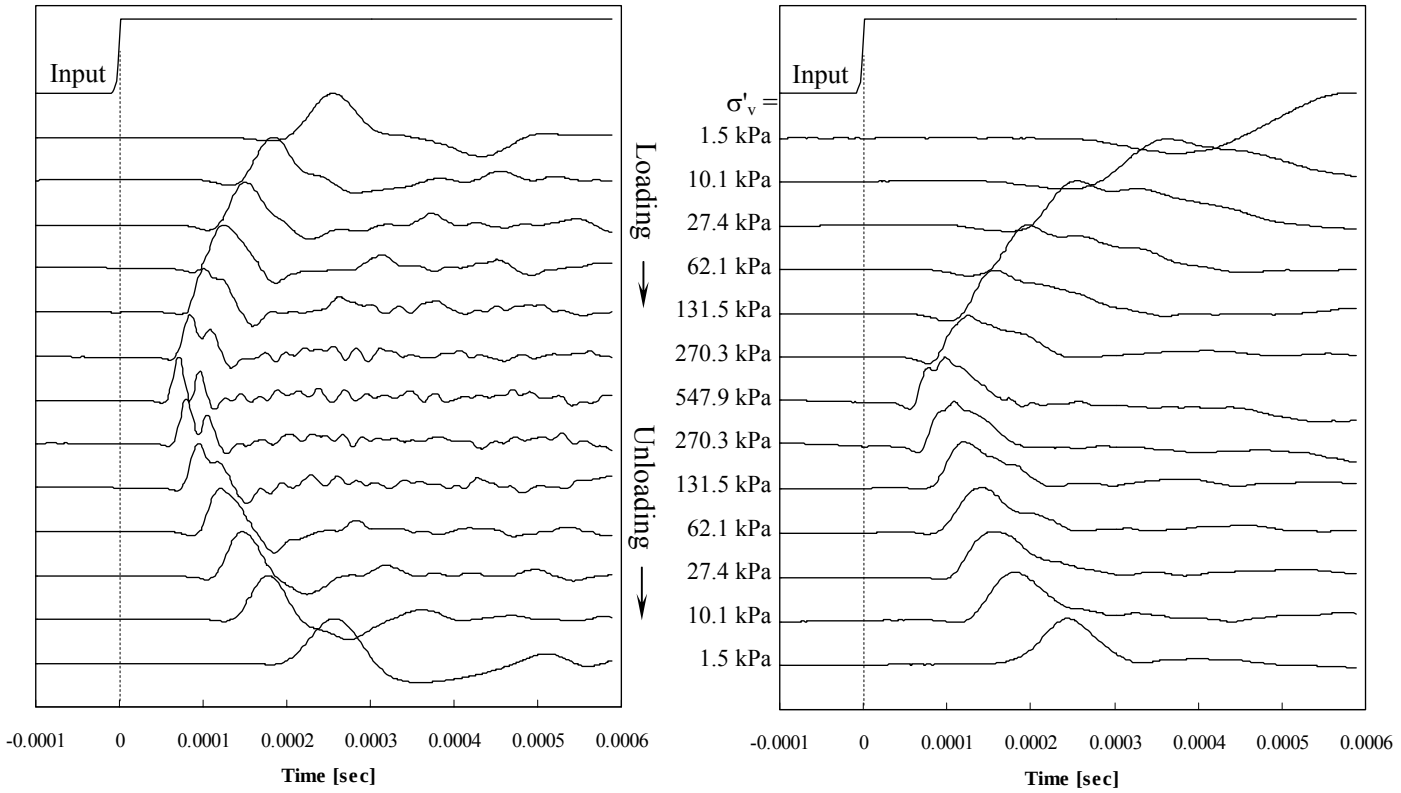

(a) Ottawa sand (R = 0.8, S = 0.9)

(b) Crushed sand 2Z8 (R = 0.1, S = 0.6)

Fig. 4. Shear wave time series gathered at different vertical effective confining stresses during loading and unloading in an instrumented oedometer cell (Additional properties for these sands can be found in Table A1).

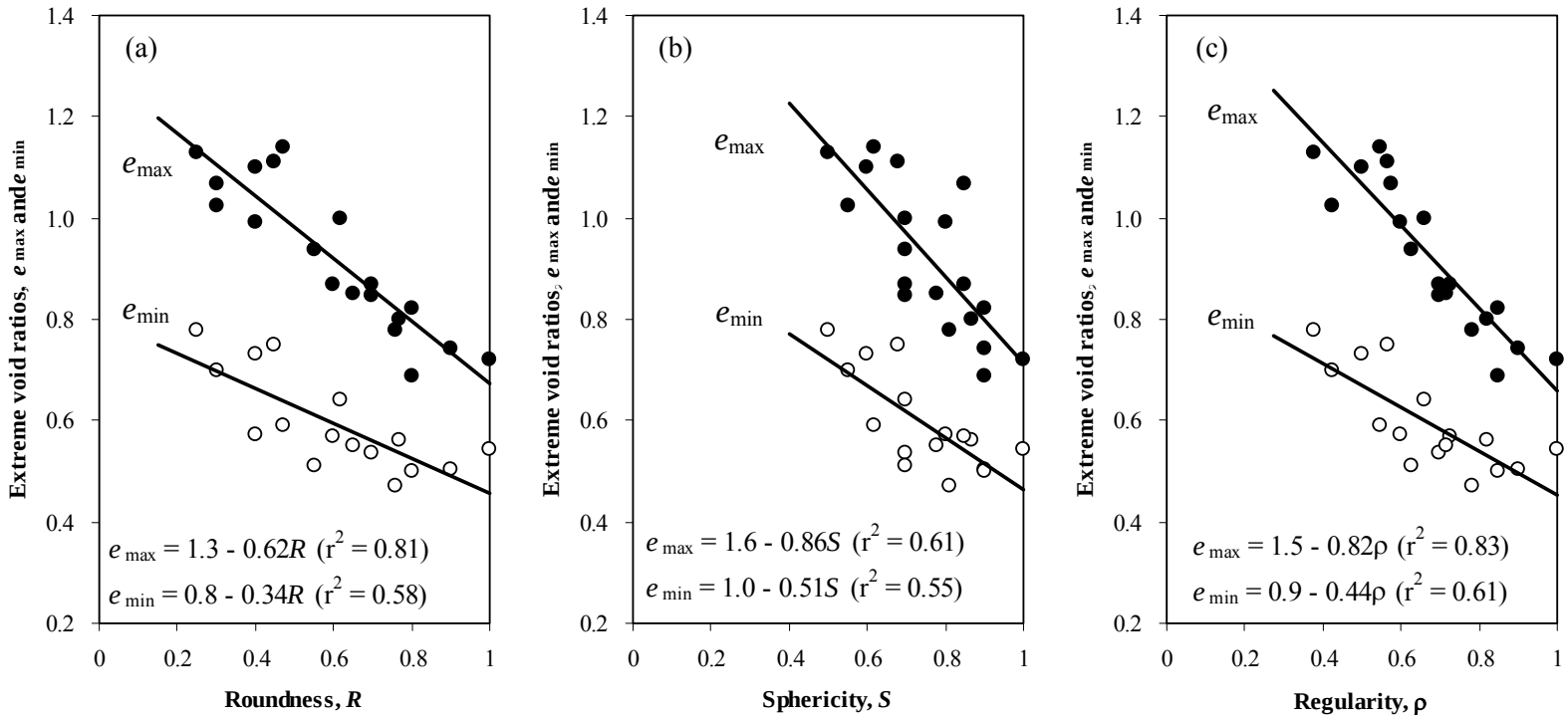

Fig. 5. Effect of particle shape on extreme void ratios (natural sands with $C_u \leq 2.5$ - Data in Table A1).

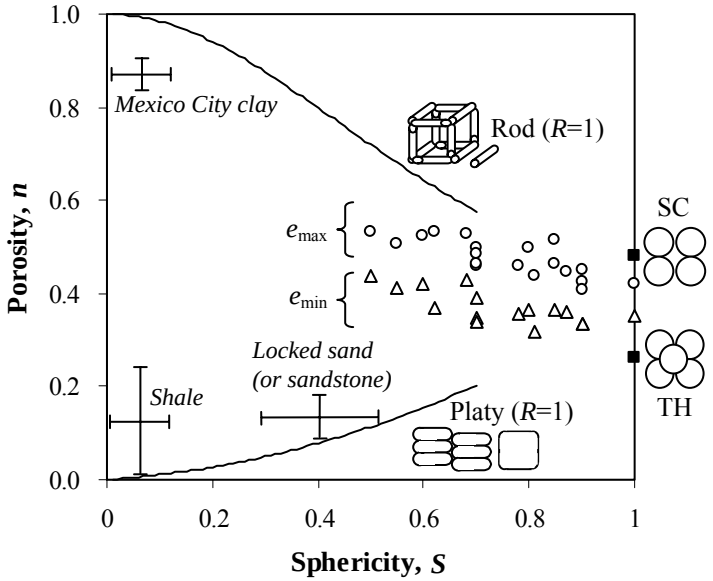

Fig. 6. Variation of porosity with sphericity. Trends: geometric analysis based on the extreme packings shown in the figure (particles remain round R=1). Data points: natural sands (this study - Table A1). Extreme values at S=1 correspond to simple cubic SC packing, tetrahedral TH packing, and experimental data with glass beads. Ranges: from published studies.

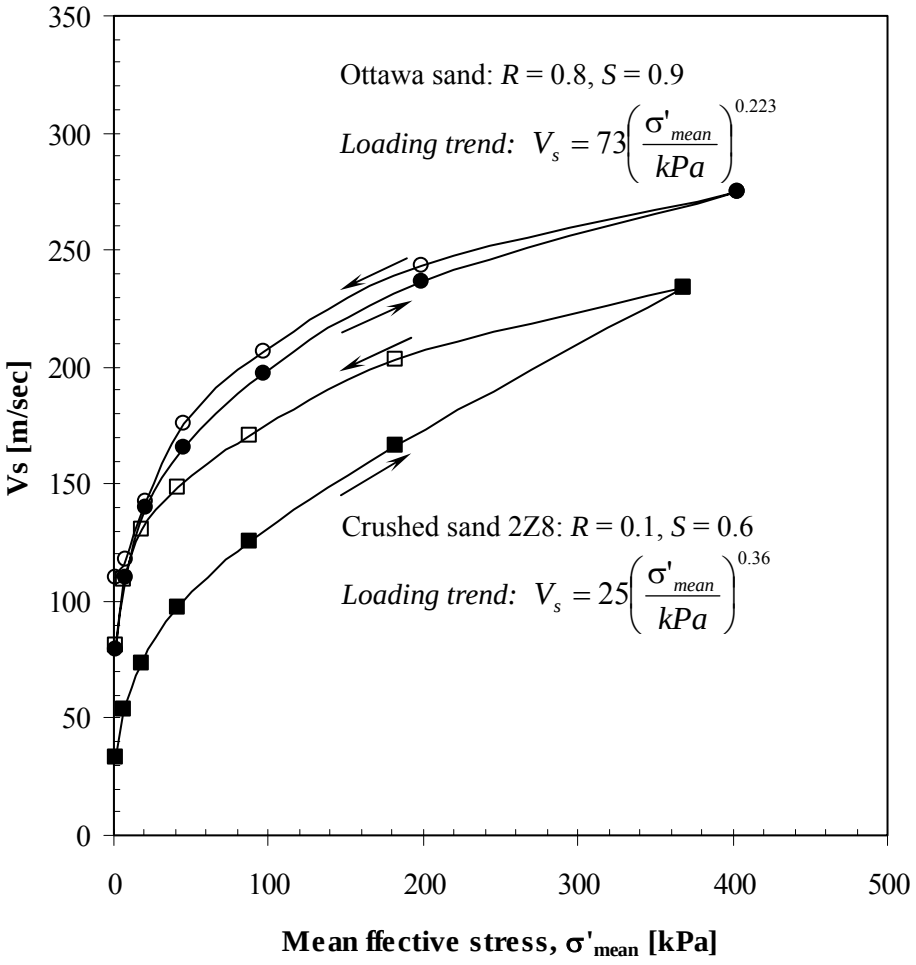

Fig. 7. Variation of shear wave velocity with effective confining stress (Refer to Fig. 4 – additional properties for these sands can be found in Table A1).

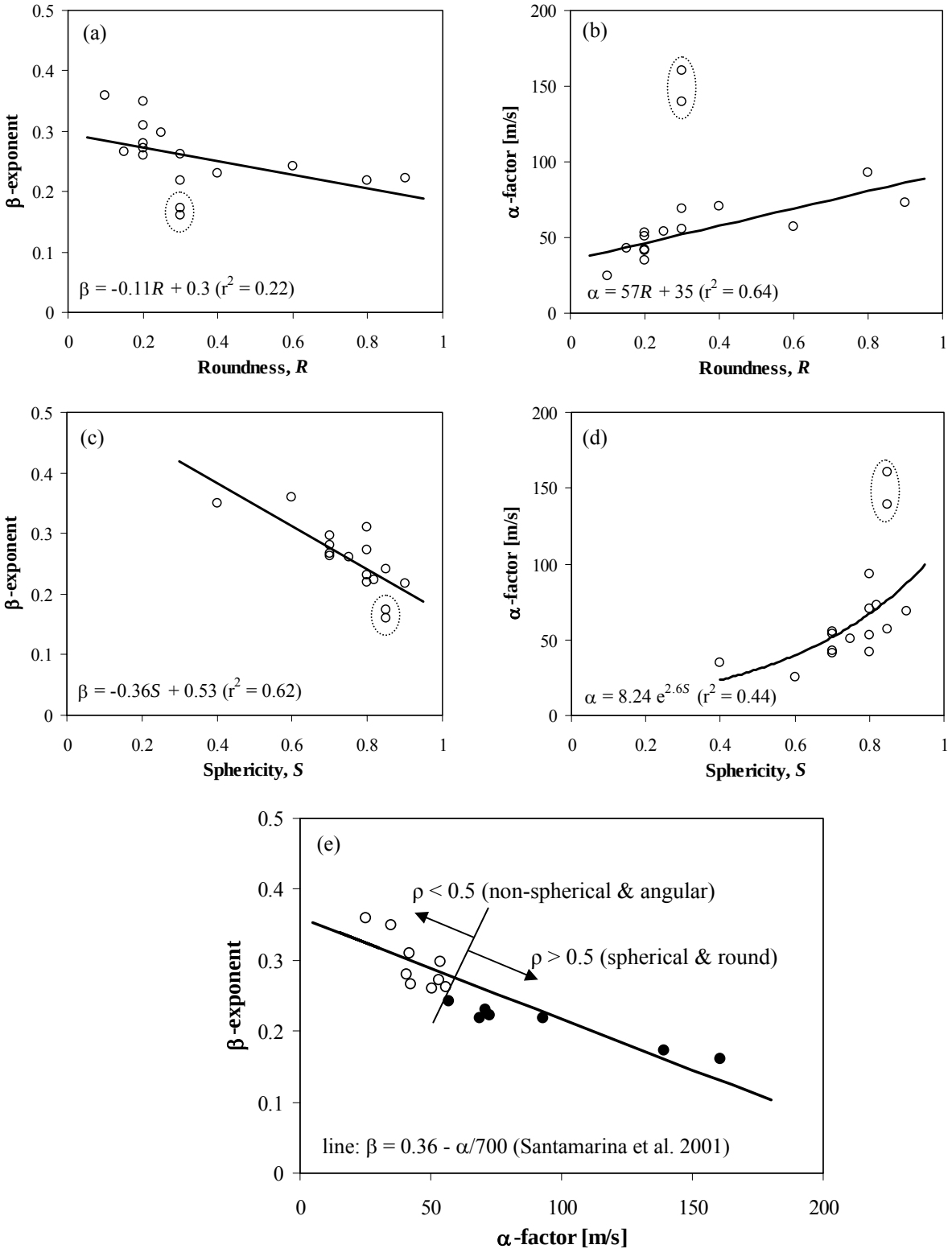

Fig. 8. The effect of particle shape on small-strain shear wave velocity (data in Table A1). The two encircled points in Fig. 8(a~d) correspond to Ponte Vedra and Jekyll Island sands which contain a high percentage of crushed shells.

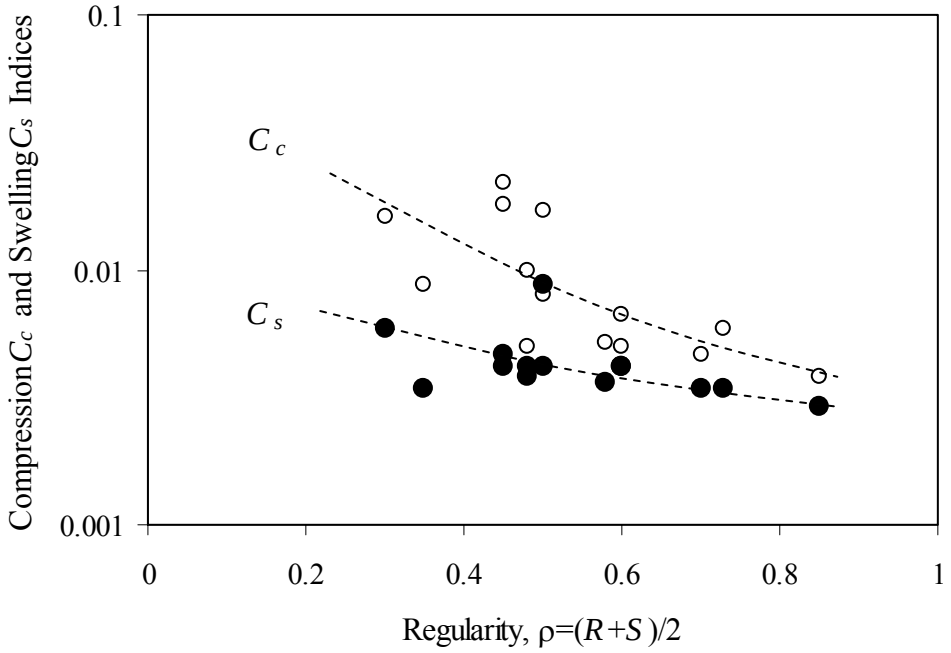

Fig. 9. The effect of particle shape on zero-lateral strain oedometric stiffness during compression and expansion (data in Table A1).

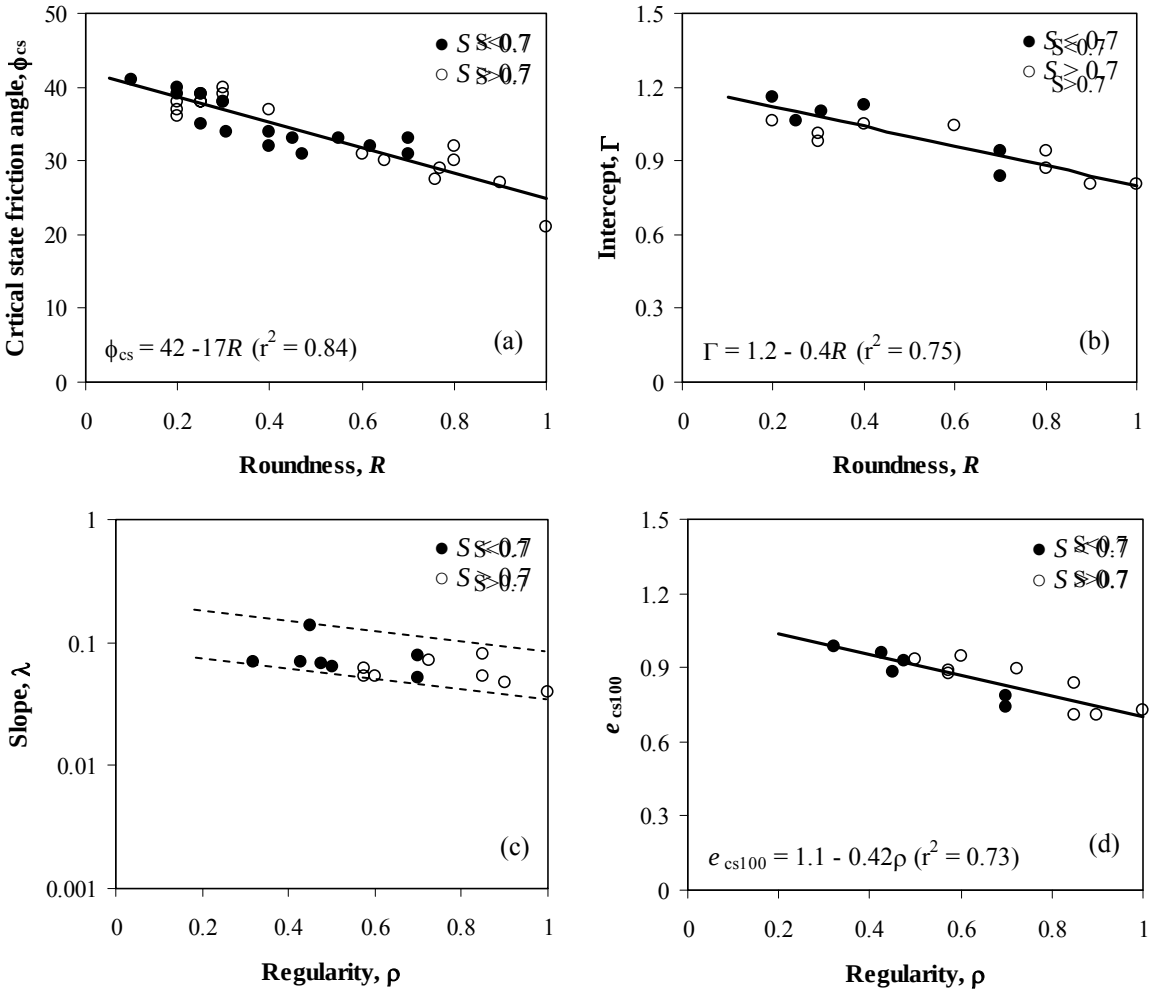

Fig. 10. The effect of particle shape on critical state parameters (data in Table A1).

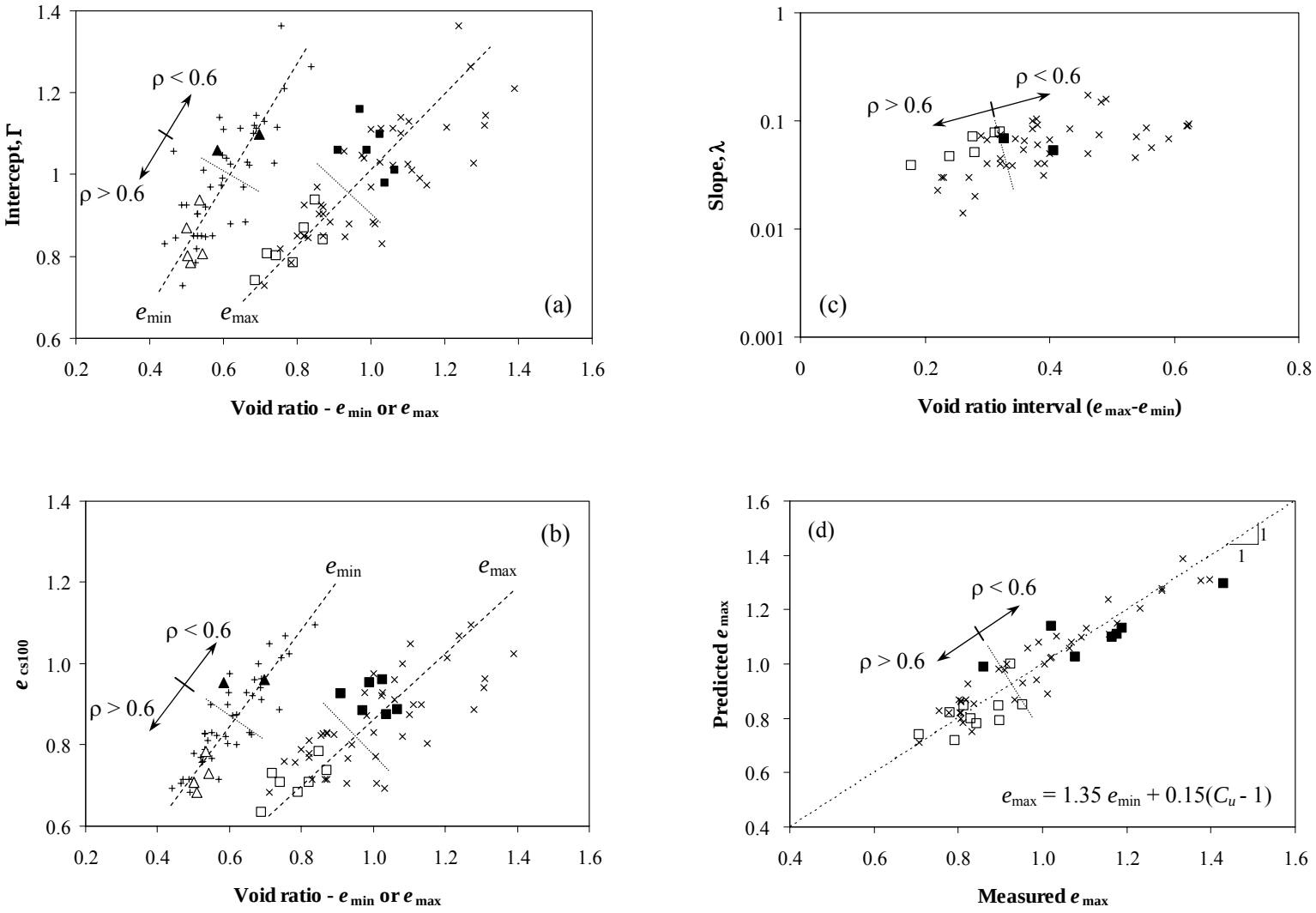

Fig. 11. Correlations between parameters (data in Tables A1 and A2).

Table A1. Database compiled from new experiments (includes particle shape information).

Soil Type	Gradation		Particle Shape			Packing		CS parameters			K_o loading		V_s-σ relation	
	D_{50}	C_u	R	S	ρ	e_{max}	e_{min}	ϕ_{cs}°	Γ	λ	C_c	C_s	α	β
Nevada sand	0.15	1.8	0.60	0.85	0.73	0.850	0.570	31	1.040	0.071	0.0059	0.0034	56.8	0.242
Ticino sand	0.58	1.5	0.40	0.80	0.60	0.990	0.574	37	1.050	0.053	0.0050	0.0042	70.7	0.231
Margaret river sand [1)]	0.49	1.9	0.70	0.70	0.70	0.870		33	0.840	0.051	0.0046	0.0034	93.2	0.219
Ottawa sand	0.60	1.4	0.80	0.90	0.85	0.690		32	0.740	0.053	0.0038	0.0029	72.7	0.223
Ponte Vedra sand [2)]	0.18	1.8	0.30	0.85	0.58	1.070		39	1.010	0.061	0.0052	0.0036	160.6	0.161
8M8-crushed sand	0.38	3.3	0.20	0.70	0.45	0.970		40	1.160	0.138	0.0220	0.0042	55.7	0.262
9C1-crushed sand	0.52	2.3	0.25	0.70	0.48	0.910		39	1.060	0.067	0.0050	0.0038	54.0	0.297
Jekyll island sand [2)]	0.17	1.7	0.30	0.85	0.58	1.040		40	0.980	0.053			139.5	0.173
ASTM graded sand	0.35	1.7	0.80	0.90	0.85	0.820	0.500	30	0.869	0.080				
Blasting sand	0.71	1.9	0.30	0.55	0.43	1.025	0.698	34	1.099	0.069				
Glass beads	0.32	1.4	1.00	1.00	1.00	0.720	0.542	21	0.807	0.039				
Granite powder	0.09	6.2	0.40	0.24	0.32	1.296	0.482	34	1.124	0.070				
Ottawa #20/30 sand	0.72	1.2	0.90	0.90	0.90	0.742	0.502	27	0.802	0.047				
Ottawa F-110 sand	0.12	1.7	0.70	0.70	0.70	0.848	0.535	31	0.937	0.077				
7U7-crushed sand	0.30	3.2	0.20	0.80	0.50	0.790		37	1.060	0.064				
1K9-crushed sand	0.30	3.4	0.20	0.40	0.30	1.160		39			0.0160	0.0059	35.0	0.350
2Z8-crushed sand	0.48	5.0	0.10	0.60	0.35	0.860		41			0.0088	0.0034	25.0	0.360
5Z9-crushed sand	0.40	3.6	0.30	0.90	0.60	0.890		38			0.0067	0.0042	68.9	0.218
6H1-crushed sand	0.33	3.8	0.20	0.80	0.50	0.970		38			0.0170	0.0088	53.0	0.272
9F1-crushed sand	0.33	3.5	0.20	0.80	0.50	0.900		36			0.0080	0.0042	41.8	0.310
3P3-crushed sand	0.27	2.2	0.20	0.70	0.45	0.950					0.0180	0.0046	41.0	0.280
6A2-crushed sand	0.33	5.5	0.20	0.75	0.48	0.930					0.0100	0.0042	50.8	0.260
5U1-crushed sand	0.32	3.5	0.15	0.70	0.43	0.840							42.6	0.266

Table A1. Continued.

Soil Type	Gradation		Particle Shape			Packing		CS parameters			K_o loading		V_s-σ relation	
	D_{50}	C_u	R	S	ρ	e_{max}	e_{min}	ϕ_{cs}	Γ	λ	C_c	C_s	α	β
Sandboil sand	0.36	2.4	0.55	0.70	0.63	0.790	0.510	33						
Daytona Beach sand [3)]	0.23	1.4	0.62	0.70	0.66	1.000	0.640	32						
Fraser River sand [3)]	0.30	1.9	0.25	0.50	0.38	1.130	0.780	35						
Michigan dune sand [3)]	0.33	1.5	0.77	0.87	0.82	0.800	0.560	29						
Ottawa #20/70 sand [3)]	0.53	2.4	0.76	0.81	0.79	0.780	0.470	28						
Ottawa #45 sand [3)]	0.57	2.1	0.45	0.68	0.57	1.110	0.750	33						
Ottawa #60/80 sand [3)]	0.21	2.4	0.65	0.78	0.72	0.850	0.550	30						
Ottawa #90 sand [3)]	0.27	2.2	0.40	0.60	0.50	1.100	0.730	32						
Syncrude Tailings [3)]	0.18	2.5	0.47	0.62	0.55	1.140	0.590	31						
1O2-crushed sand	0.25	2.9	0.25	0.80	0.53	0.830		38						
1O6-crushed sand	0.21	2.8	0.30	0.70	0.50	0.770		38						
6F5-crushed sand	0.25	3.3	0.25	0.80	0.53	0.910		39						
8B8-crushed sand	0.32	3.7	0.25	0.80	0.53	0.850		38						
3C7-crushed sand	0.26	3.2	0.25	0.80	0.53	0.850								
2L6-crushed sand	0.28	3.5	0.25	0.80	0.53	0.840								

Note: [1)] Its texture is very smooth; [2)] They contain a high percentage of crushed shells (flaty particles); [3)] Data are extracted from the study by Sukumaran and Ashmawy (2001) and Ashmawy et al. (2003).

Notation: D_{50} mean size [mm], C_u coefficient of uniformity, R roundness, S sphericity, ρ regularity = $(R+S)/2$, α shear wave velocity [m/s] at σ=1kPa, β slope of V_s-σ relation, C_c compression index, C_s expansion index, and ϕ_{cs}, Γ, λ critical state parameters.

Table A2. Material properties for sandy soils compiled from published studies.

Sand Type (% fines)	Gradation		Packing		CS parameters			Test condition	References
	D_{50} (mm)	C_u	e_{max}	e_{min}	$\phi_{cs}°$	λ	Γ		
Banding 1 (0%)	0.18	1.5	0.820	0.540	32	0.020	0.850	CU	Castro et al. (1982), Sladen et al. (1985)
Banding 5 (0%)	0.11	1.4	0.870	0.550	30	0.045	0.920	CU	
Banding 6 (0%)	0.16	1.7	0.820	0.520	28.6	0.040	0.850	CU	
Banding 9 (0%)	0.14	1.6	0.800	0.530	26.8	0.030	0.850	CU	
Brenda (0%)	0.10	1.9	1.060	0.688	36	0.100	1.112	CU	Robertson et al. (1995)
Chiba (3%)*	0.17	2.0	1.271	0.839	34	0.085	1.265	CU	Ishihara (1993)
Chiba (18%)*	0.15	4.0	1.307	0.685	34	0.090	1.120	CU	
Chonan Silty (18%)	0.15	4.1	1.310	0.690	34	0.090	1.144	CU	
Dune (6%)*	0.21	2.3	1.080	0.590	32	0.159	1.139	CU	Konrad (1990)
Erksak 330 (0.7%)	0.33	1.8	0.753	0.527	31	0.030	0.820	CD & CU	Konrad and Watts (1995)
Fort Peck (2%)*	--	--	1.010	--	32	0.087	0.879	CU	Been et al. (1991)
Fraser River (0%)	0.25	1.7	1.000	0.6	34.5	0.067	1.110	CU	Chillarige et al. (1997)
Hostun RF (0%)	0.32	1.8	1.000	0.655	33.5	0.069	0.969	CU	Thevanayagam et al. (1996), Gajo and Wood (1999)
Kiyosu (0%)*	0.31	2.5	1.206	0.745	30	0.050	1.115	CU	Ishihara (1993)
Kogyuk 350 (0%)	0.35	1.7	0.783	0.523	31	0.014	0.784	CU	Been and Jefferies (1985)
Kogyuk 350 (2%)	0.35	1.8	0.829	0.470	31	0.065	0.845	CU	
Kogyuk 350 (5%)	0.36	2.0	0.866	0.487	31	0.105	0.925	CU	
Kogyuk 350 (10%)	0.34	2.3	0.927	0.465	31	0.175	1.056	CU	
Lagunillas (70%)	0.05	3.0	1.389	0.766	31	0.093	1.210	CU	Ishihara (1993)
Leighton Buzzard (5%)	0.12	1.8	1.023	0.665	30	0.054	1.030	CU	Been et al. (1991)
Likan (0%)	0.24	1.9	1.239	0.756	34.5	0.148	1.364	CD & CU	Lee (1995)
Lornex (0%)	0.30	2.0	1.080	0.680	35	0.050	1.100	CU	Castro et al. (1982), Sasitharan et al. (1994)
Mailiao (5%)	0.25	2.9	1.279	0.739	--	0.071	1.029	CU	Chen and Liao (1999)
Mailiao (10%)	0.22	3.5	1.151	0.595	--	0.086	0.975	CU	

Table A2. Continued.

Sand Type (% fines)	Gradation		Packing		CS parameters			Test condition	References
	D_{50} (mm)	C_u	e_{max}	e_{min}	$\phi_{cs}°$	λ	Γ		
Mailiao (15%)	0.21	4.2	1.031	0.440	--	0.068	0.830	CU	Chen and Liao (1999)
Massey tunnel (3%)	0.25	1.5	1.102	0.710	39.5	0.040	1.129	CU	Konrad (1997)
Monterey (0%)*	0.38	1.6	0.860	0.530	33	0.039	0.905	CD & CU	Riemer et al. (1990), Riemer and Seed (1997)
Monterey (16%)*	1.30	1.3	0.710	0.490	33	0.023	0.730	CU	
Nerlerk (0%)	0.23	1.8	0.890	0.660	30	0.030	0.885	CU	Sladen et al. (1985)
Nerlerk (2%)	0.23	2.0	0.940	0.620	30	0.040	0.880	CU	
Nevada fine (5%)	0.12	1.8	0.870	0.570	29	0.067	0.850	CU	Arulanandan et al. (1993)
Ottawa (5%)	--	--	--	--	29.5	0.067	0.809	CU	Cunning et al. (1995), Sasitharan et al. (1994)
Ottawa C109 (0%)	0.35	1.7	0.820	0.500	30	0.074	0.926	CU	
S (12%)	0.80	3.0	1.133	0.596	39	0.046	0.992	CU	Verdugo et al. (1995)
S (20%)	0.70	3.8	1.111	0.547	38	0.056	1.012	CU	
Sacramento (0%)	0.30	1.7	0.870	0.530	33.2	0.039	0.905	CU	Riemer et al. (1990), Riemer and Seed (1997)
Sand A (13%)	0.14	2.9	--	--	33.7	0.120	1.071	CU	Dobry et al. (1985)
Sand B (32%)	0.09	3.3	--	--	33.7	0.045	0.972	CU	
Sydney (0%)	0.30	1.5	0.855	0.565	31	0.073	0.969	CD & CU	Chu & Lo (1993)
Syncrude (12%)	0.17	2.4	0.930	0.550	30	0.040	0.847	CU	Sladen & Hanford (1987), Cunning et al. (1995)
Tar Island Dyke (5%)*	--	--	1.005	--	--	0.057	0.885	CU	Konrad and Watts (1995)
Tia Juana Silty (12%)	0.16	2.7	1.099	0.620	30.5	0.075	1.026	CU	Ishihara (1993)
Toyoura (0%)	0.17	1.7	0.977	0.597	31	0.060	1.048	CU	Ishihara (1993), Toki et al. (1986)
Toyoura (0%)	0.16	1.5	0.981	0.608	31	0.084	1.041	CU	Been et al. (1991)
Unimin 2010 (0%)	0.87	2.0	1.027	0.646	33	0.091	1.112	CU	Zhang & Garga (1997)
Well-rounded (1%)	0.18	1.4	1.060	0.670	31	0.031	1.022	CU	Konrad (1990)

Note: The stress range for the critical state parameters is $p'_{cs} < \sim 400$ kPa; the CU and CD in test condition are conventional consolidated undrained and drained tests respectively. * Critical state parameters are based on quasi-steady and steady state conditions.